JOURNAL OF PROPULSION AND POWER
Vol. 17, No. 2, March–April 2001

Reaction and Mixing-Controlled Combustion in Scramjet Engines

Tohru Mitani,* Nobuo Chinzei,† and Takeshi Kanda‡
National Aerospace Laboratory, Kakuda Research Center, Kakuda, Miyagi 981-1525, Japan

H_2-fueled scramjet engines were tested under Mach 4 ($M4$) to Mach 8 ($M8$) flight conditions, and the local equivalence ratio and combustion efficiency were measured by gas sampling at the engine exit. Correlation between the local values of equivalence ratio and combustion efficiency showed that the $M4$ combustion was principally reaction controlled and the reaction and the mixing-controlled combustion coexisted in the $M6$ condition. The $M8$ combustion in the engines was rate controlled by the mixing of H_2. Comparison of engine performance in the air, supplied by a combustion heater and a storage heater, indicated that the performance strongly depended on the air-heating methods. The dependence of engine performance on air-heating methods could be explained by the finding that the $M6$ engine combustion was partially reaction controlled. The wall-heating rate and pressure distribution in the $M6$ tests also supported the shift from the partially reaction-controlled to the mixing-controlled combustion as the fuel rate was increased. The mixing-controlled combustion suggested weak facility dependence in the $M8$ condition. Because reaction in the $M8$ condition is not sufficiently fast, the main combustion region might be blown downstream in the engine.

Nomenclature

H	=	height of the engine (250 mm)
k_1	=	reaction rate of the reaction $H + O_2 \rightarrow OH + H$
M	=	Mach number
n	=	pressure exponent in Eq. (3) (order of overall reactions)
P_b	=	typical burning (static) pressure weight-averaged with $n = 1.6$
P_i	=	typical ignition (static) pressure weight-averaged with $n = 1$
P_w	=	wall pressure
S	=	heated by a storage air heater
T_r	=	recovery temperature in engines
t_b	=	burning time of H_2 in engines (assumed to be t_{95})
t_{flow}	=	residence time in the burning length, x_e
t_{ig}	=	ignition time defined as $10 \times t_1$
t_s	=	typical gas sampling time (1.5 s)
t_1	=	characteristic time defined as $(k_1[O_2])^{-1}$
t_{95}	=	reaction time to raise the temperature from 5 to 95% of the equilibrium temperature rise
U	=	typical flow velocity in engines
V	=	heated by a vitiation air heater
x_b	=	characteristic length required to burn fuel
x_e	=	burning length in engines (1.3 m)
x_{ig}	=	characteristic length required to ignite fuel
Φ	=	bulk fuel equivalence ratio supplied to engines
ϕ	=	local fuel equivalence ratio (time-averaged, if not specified)
η_c	=	local combustion efficiency (time-averaged, if not specified)
-	=	time- or space-averaged values

Introduction

HYPERSONIC wind tunnels require high-temperature test air to simulate scramjet inlet or combustor inlet conditions. Combustion heaters (often called vitiation air heaters) produce H_2O and radicals, and arc heaters supply large amounts of NO. The effects of test facility contamination have long been a concern in hypersonic propulsion research. Many chemical kinetic studies on the vitiated air effect have been reported.[1–5] However, few experimental works have been reported on the sensitivity of scramjet performance to the test air. Only one engine data set, reported by Guy et al.,[6] on air source exists. They reported that the thrust in the arc-heated air was significantly higher than in the vitiated air. The facility dependence of engine test results is still an open question and concern.[7,8]

A ramjet engine test facility (RJTF) was constructed in the National Aerospace Laboratory of Japan. The review of RJTF and engine tests to date are documented in Ref. 9. In the RJTF, either a storage air heater (SAH: S) or a vitiation air heater (VAH: V) can be chosen for $M6$ engine testing to raise the air temperature to 1500 K. Comparative experiments of scramjet engines were conducted in both $M6S$ and $M6V$ test air. The results showed that the ignition and the thrust (combustion) performance indicated particular sensitivities to the air.[10] It is necessary to investigate rate processes governing the overall combustion rates to understand this facility dependence.

In this study, global rate processes in the engine combustion in the $M4$, $M6$, and $M8$ conditions are first discussed using local equivalence ratio (ϕ) and combustion efficiency (η_c). Correlation between ϕ and η_c clarifies the shift of the reaction-controlled combustion in the $M4$ to the mixing-control combustion in the $M8$ condition. Coexistence of the reaction and the mixing-control combustion explains the facility dependence of engine performance in the $M6$ case, which is also supported by the observations of wall-heating rate and pressure distributions. Reaction times of ignition and engine combustion as well as the reaction environment of engines are evaluated to identify the features of automatic ignition and burning under the scramjet engine conditions.

Scramjet Engine and Measurements

Scramjet Engines Tested

The scramjet engine tested in the present study is shown in Fig. 1. The rectangular engine, with a length of 2.1 m, consists of the cowl, the top wall, and two sidewalls. The entrance and the exit of the engine are 200 mm wide × 250 mm high (which is denoted by H). There are two engines with the same internal and external geometries: an uncooled, heat-sink-type engine for the $M4$ and $M6$ testing and a water-cooled engine for the $M8$ testing. Details of the engines are found in Refs. 9 and 11.

The inlet is a sidewall compression type with a 6 deg half-angle. The leading edge is swept back by 45 deg to deflect airstream for the

Received 1 July 1999; revision received 1 June 2000; accepted for publication 25 August 2000.

*Head of Ramjet Combustion Laboratory, Ramjet Division, Kimigaya 1; mitani@kakuda-splab.go.jp.
†Director of Ramjet Division, Ramjet Division, Kimigaya 1.
‡Head of Ramjet System Laboratory, Ramjet Division, Kimigaya 1.

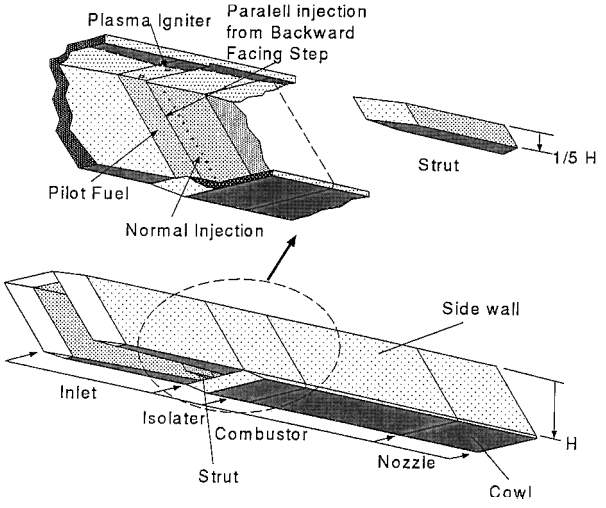

Fig. 1 H_2-fueled scramjet engines tested in the RJTF.

suitable spillage required for starting. The geometrical contraction ratio is 2.86 without a strut. Ducts with a constant cross-section (isolator) are installed between the inlet and the combustor. Two kinds of isolators, 100 and 200 mm long, were tested to investigate the effects to engine unstart due to combustion.

Results for Engine Geometries Without Struts and Three Kinds of Struts

A 50-mm-high ($1/5H$), 30-mm-thick strut and a 250-mm-high ($5/5H$) struts with 30 and 46 mm thickness are presented here. Two 2.5-kW plasma jet (PJ) igniters are assembled in engines in the $M4$ and $M6$ tests.[9–12] Backward-facing steps between the isolator and the combustor were used for flame holding. Their heights are 4 mm on the sidewalls and 2 mm on the top wall. The main H_2 is injected normal to the flow from the sidewalls through 24 holes in the combustor. There is no fuel injection from the strut. The stoichiometric H_2 flow rates are 190 g/s ($M4$), 140 g/s ($M6$), and 48 g/s ($M8$), which were evaluated from the air capture ratios of 0.72 ($M4$), 0.85 ($M6$), and 0.87 ($M8$). The capture ratios were determined by metering the air mass flow rates with choked orifices in subscale models. The inner surface of the top wall of the engine was leveled to the lower surface of the facility nozzles to simulate the boundary-layer ingestion of scramjet engines.

Measurements and Procedure

Thrust, lift, and pitching moment delivered by engines were measured by a floating-frame force measuring system. The forces were compared with those obtained by the integration of wall pressure measured at 150 locations. The engine wall temperature was monitored by using thermocouples, embedded 1 mm deep from the inner surface at 40 stations in the heat-sink-type engine to estimate the local heat flux to the engine.[12]

The local equivalence ratio (ϕ) and the local combustion efficiency (η_c) are much more informative in elucidating mixing schedule and progress of combustion in supersonic combustion engines. Gas sampling and pitot pressure measurements were made at about 70 stations across the exit plane, 5 mm downstream of engine with three water-cooled, 12-probe rakes. Gas chromatography was used to measure the amounts of H_2, O_2, and N_2 (Ref. 10).

Accuracy of measurements of pressure and gas composition is better than 1% because they are calibrated before the experiments. The accuracy of ϕ does not depend on the quenching of sampled gas. The combustion efficiency measured by gas sampling is based on the assumption that gas composition is preserved in the sampling process. The airflow rate and the H_2 fuel rate measured at the engine exit were compared with their supply rates to examine the quenching of sampled gas. In the experiments, deficient mass flux of air of about 15% was observed in the mass flux derived by integration across the engine exit. This discrepancy was caused by overestimation of the total temperature. The higher temperature was attributed to the negligence of heat loss in engines and partially to insufficient quenching of the gas-sampling probes. However, quenching of the H_2 and O_2 mixture, even in airflow with $T_0 = 2600$ K, was confirmed in an $M8$, accidentally unstart experiment, where gas-sampling data gave lower η_c, from 30 to 95%. Our validation study of quenching[13] and sensitivity analysis[14] also indicated that the end-to-end uncertainty, including the repeatability of experiments, of the rake probing was smaller than ±5%.

Correlation Between ϕ and η_c

Rate Processes and Combustion Efficiency

Typical results of ϕ and η_c measured at the engine exit are illustrated in Figs. 2a and 2b for $M8$ tests (the bulk $\Phi = 0.7$) installing the thick, $5/5H$ strut (46 mm thick and 250 mm high).[15] The top wall is located on the upper side, and the cowl is on the lower side of the figures. The z axis is in the spanwise direction of the engine exit. A fuel-rich region with $\phi = 0.9$ is found in the center, near the top wall, and the cowl side is occupied by a lean region of $\phi = 0.3$. The local mass flux of air indicates distorted air to the cowl side because the airflow is deflected to the cowl by the swept-back inlet. This deflection can be observed more clearly in the $M4$ case shown later, in Fig. 4. The H_2 flux distribution shows that H_2 is concentrated near the top wall in spite of the uniformly distributed injection holes on the side walls. Our oil flow experiments indicated that the H_2 distorted near the top wall was carried with the core flow deflected in the swept-back diverging combustor.

The local η_c is illustrated in Fig. 2b. A higher η_c is located near the cowl side, and a lower η_c is found near the top wall. (The mass-flux-averaged η_c gives a fairly high bulk η_c above 85%.) This tendency of higher η_c near the cowl is opposite to that found in the $M4$ testing (Fig. 4b). When these ϕ and η_c are compared, locations near the stoichiometric condition ($\phi = 1$) have lower η_c and vice versa. This tendency was observed in the $M6$ tests with higher bulk combustion efficiencies and in component tests using a direct-connect

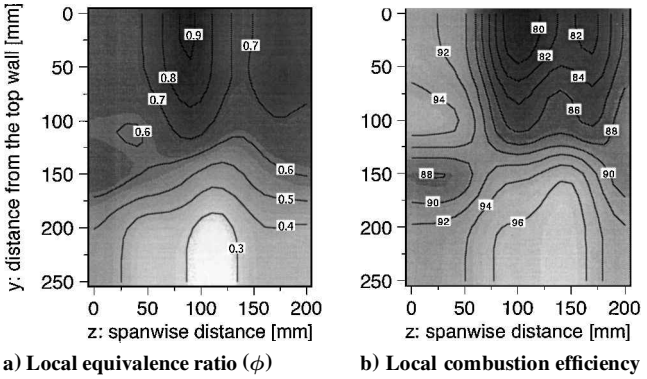

a) Local equivalence ratio (ϕ) **b) Local combustion efficiency (η_c)**

Fig. 2 Local combustion performance measured at the engine exit (an engine configuration with the 100 mm isolator and the 46-mm-thick 5/5H strut in $M8$.

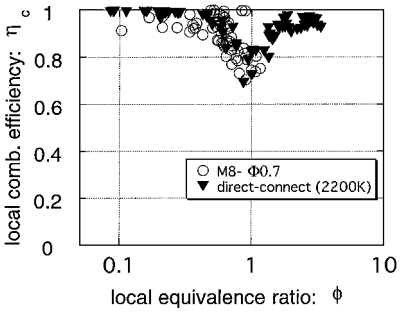

Fig. 3 Correlation between ϕ and η_c in the $M8$ engine and direct-connect combustor tests.

Table 1 Comparison of engine performance ($M6$)

Test air-heating modes	Storage-heated	Vitiation-heated
Autoignition without preheating	Impossible	Possible
Autoignition with preheating	Marginal	Possible
Flame holding without PJ igniters	Marginal	Good
With strut	Poor	Marginal
In weak combustion mode	Marginal	Fair
Limit fuel rate causing unstart	60 g/s ($\Phi = 0.4$)	100 g/s ($\Phi = 0.7$)

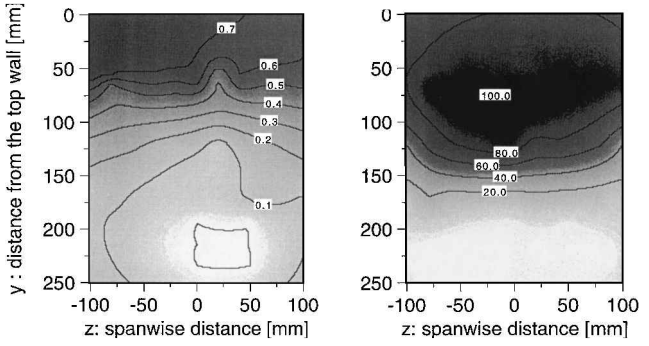

a) Local equivalence ratio (ϕ) **b) Local combustion efficiency (η_c)**

Fig. 4 Local combustion performance measured at the engine exit (an engine configuration with the 200 mm isolator without a strut in $M4$).

supersonic combustor. These observations help to clarify the rate processes in the engine.

At the engine exit, lean and rich reactants are carried by turbulent eddies in engines. The typical gas-sampling time (t_s, 1.5 s) is sufficiently long compared to the times of fluctuation due to turbulence (typically $H/U \sim 0.1$ ms). The local, time-averaged equivalence ratio is defined as

$$\bar{\phi}(y, z) = \int_0^{t_s} \frac{\phi(t: y, z)\, \mathrm{d}t}{t_s} \tag{1}$$

The maximum combustible H_2 for the time-averaged ϕ is expressed using the minimum function, $\min(\bar{\phi}, 1)$. The combustion efficiency is defined as the ratio between actually burned fuel and the combustible fuel. At the limit of mixing-controlled combustion, instantaneous, maximum combustible H_2 is given by $\min(\phi, 1)$ for fluctuating $\phi(t)$. Consequently, the combustion efficiency measured by the sampled gas can be written as

$$\bar{\eta}_c(y, z) = \int_0^{t_s} \frac{\min\{\phi(t: y, z), 1\}\, \mathrm{d}t}{\{\min(\bar{\phi}, 1) \cdot t_s\}} \tag{2}$$

This implies that excess H_2, when $\phi(t) > 1$, and excess O_2, when $\phi(t) < 1$, are sampled during a gas-sampling time t_s. They are eventually mixed with each other in a sampling bottle to lead to a lower $\bar{\eta}_c$. This effect becomes most pronounced for the stoichiometric reactant and the time-averaged $\bar{\eta}_c$ decreases near $\bar{\phi} = 1$. When a $\bar{\phi}$-$\bar{\eta}_c$ diagram is plotted, the $\bar{\eta}_c$ has a lower value, near $\bar{\phi} = 1$, and it approaches $\bar{\eta}_c = 1$ under the far stoichiometric conditions in the mixing-controlled combustion. The depth and the extent of the dip depend on the mixing (turbulence) properties in the internal flow in the engines. Small eddies reduce the size of dip. This mixing-controlling limit yields the upper bound of $\bar{\eta}_c$.

The other limit, the complete mixing of fuel, is impossible in scramjet engines because typical flow velocities are from 900 m/s ($M4$) to 2000 m/s ($M8$), the residence times range from 1 to 0.5 ms in the combustor (presented later, in Table 2). In this limit, a spectrum line appears at the location corresponding to the bulk Φ in the $\bar{\phi}$-$\bar{\eta}_c$ diagram. The poor mixing of H_2 in the engine yields horizontal dispersion and the reaction delay causes vertical dispersion of the data. When overall the combustion rate is controlled by mixing and reaction, the data must disperse widely without any correlation in

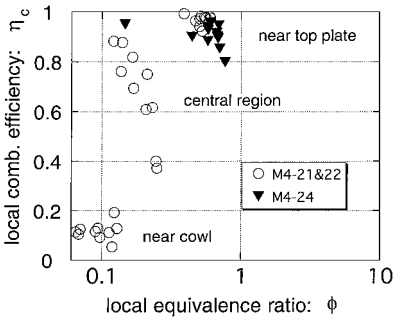

Fig. 5 Correlation between ϕ and η_c in the $M4$ engine tests (an engine configuration with the 200 mm isolator without struts).

the $\bar{\phi}$-$\bar{\eta}_c$ diagram. Hereafter, the time-averaged ϕ and η_c are denoted by simply ϕ and η_c.

Rate Process in the $M8$ Combustion

The higher combustion efficiency shown in Fig. 2b is not always found in the $M8$ tests. For instance, the engine configuration without the struts could not hold flame in the combustor.[16] An engine configuration with a thin (30-mm-wide) strut delivered lower thrust, which might be caused by the poor flame-holding characteristic of the strut.[17] The higher combustion performance illustrated in Fig. 2b is attributed to a thicker (46-mm-wide) strut in the tests.

Figure 3 illustrates a correlation between ϕ and η_c, in which the open circles denote the data shown in Fig. 2 and the solid triangles are data obtained in direct-connect combustor tests. The direct-connect combustor data were derived in experiments under mixing-controlled conditions and clearly show the dip at $\phi = 1$. The circles align with the data denoted by the triangles, implying that the $M8$ combustion in the engine with the thick strut is primarily rate controlled by fuel mixing.

Rate Process in the $M4$ Combustion

Results of ϕ and η_c obtained in an $M4$ condition ($\Phi = 0.27$) without the struts are illustrated in Fig. 4a and 4b (Ref. 18). A fuel-rich region with $\phi = 0.7$ is found near the top wall, and the cowl side is occupied by an H_2-free region. The local η_c in Fig. 4b illustrates that burning of H_2 is confined in the upper half, near the top plate, and the lower half of engine, near the cowl, does not burn. Comparison with Fig. 2 showed that the fuel and combustion efficiency distributed vertically in the engine without the struts. The fuel H_2 is ignited by the PJ igniters installed in the top wall. Our experiments showed that the combustion was sustained without the igniters once the ignition was attained.

The data shown in Fig. 4 is correlated with Fig. 5, in which repeatability of measurements was examined with data obtained near the top wall in a separated engine test (solid triangles). All the data are sorted into three groups: the group with high η_c found near the top wall, the group with widely scattered η_c in the central region in the engine cross-section, and the group without combustion near the cowl wall. Figure 5 shows that only the H_2 near the top wall can burn in the mixing-controlled mode. Our pitot pressure distribution studies indicated that the exhaust flow near the top plate was nearly choked at the engine exit. We expect that the mixing-controlled burning is stabilized with a large separation (subsonic) babble stationed in the combustor. The babble might occupy one-third of the flow path at the throat of the combustor section and supply heat and radicals downstream. This is why combustion is detected in the central region of the engine, as shown in Fig. 4b and Fig. 5. Similar strong interaction between the engine internal flow and combustion was observed in $M6$ tests.

The $M4$ testing shows that the flame holding is limited in the vicinity of the top wall. In designing the engines, we intended that the backward-facing step in the combustor was necessary to propagate combustion from the top wall to the cowl side. However, the poor η_c in Fig. 4b suggests an absence of a flame-holding region near the cowl. Thus, we concluded that the combustion in the $M4$

Table 2 Typical flow properties, ignition, and burning length

	P_i (kPa)	M	T_r (K)	U (m/s)	t_{ig} (s)	x_{ig} (m)	P_b (kPa)	t_b (s)	x_b (m)
$M4$	29	2	830	882	2.40×10^{-3}	2.13	85.4	2.20×10^{-4}	0.19
$M6$ without strut	15.2	4	1381	1516	1.30×10^{-4}	0.2	18.5	1.60×10^{-3}	2.49
$1/5H$—weak	14.1	3	1400	1392	1.30×10^{-4}	0.18	22.1	1.20×10^{-3}	1.69
$1/5H$—intensive	14.2	3	1400	1392	1.30×10^{-4}	0.18	63.6	2.20×10^{-4}	0.31
$M6$ with $5/5H$ strut	23.4	2	1431	1157	7.10×10^{-5}	0.08	69.2	1.90×10^{-4}	0.22
$M8$ without strut	4.3	5	2375	2087	6.20×10^{-5}	0.13	7.9	2.90×10^{-3}	5.98
$M8$ with thin $5/5H$	6.6	4	2394	1995	3.90×10^{-5}	0.08	13.7	1.20×10^{-3}	2.34

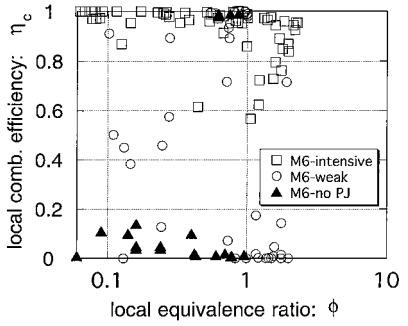

Fig. 6 Correlation between ϕ and η_c in the $M6$ engine tests (an engine configuration with the 100 mm isolator with the $1/5H$ strut).

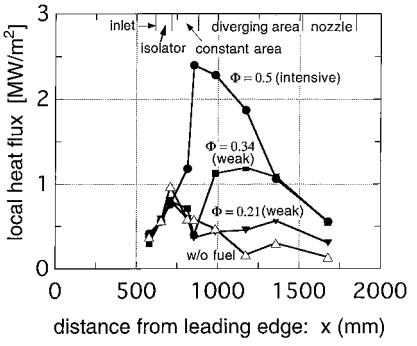

Fig. 7 Distributions of wall-heating rate in various combustion modes (the 200 mm isolator with the $5/5H$ strut in $M6S$ mode).

condition was controlled by reaction rates with the lower stagnation temperature.

Rate Process in the $M6$ Combustion

There were two combustion modes in the $M6$ engine operations, weak combustion and intensive combustion.[11] In the weak combustion mode, the thrust was small and the engine exhausted a faint plume from the nozzle exit. In the intensive combustion mode, the engine delivered a large thrust accompanied by a bright exhaust plume. The ϕ and η_c data obtained in these combustion modes are found in Figs. 6 and 7 in Ref. 10. Correlation of the data is plotted in the ϕ-η_c diagram in Fig. 6 by open squares (intensive) and open circles (weak).

The weak combustion data were widely scattered between $\eta_c = 0$ and $\eta_c = 1$, which denoted a typical reaction-controlled combustion. The burning region with higher η_c was confined in the narrow space near the top wall, and most of the H_2 was exhausted without burning. When the fuel rate increased, the weak combustion switched to the intensive combustion.

The intensive combustion data indicated higher combustion efficiency and the mixing-controlling feature. However, some of the data showing poor efficiency near $\phi = 1$ suggested that the combustion was also governed by reaction rate. Thus, in the $M6$ condition, the two processes of the reaction and the mixing-controlled combustion coexisted in the engine. Because the radicals and H_2O supplied from the VAH affect reaction rates in engine combustion, the reaction-controlled combustion may yield the dependence of engine performance in the $M6$ engine testing.

In Fig. 6, the solid triangles express the data in an "ignition failed" experiment in which the PJ igniter accidentally did not work. In the test, the force balance and the wall pressure data did not indicate any trace of combustion in the engine. In addition, most of the η_c data showed no combustion and were distributed near $\eta_c = 0$ in Fig. 6. However, three among them were observed near $\eta_c = 1$. Our study on ignition ability showed that the engine was on the self-ignition limit in the $M6$ condition. The three data near $\eta_c = 1$ suggested that H_2 was about to self-ignite without the PJ igniters in the $M6S$ mode air.

Facility Dependence in Engine Testing

Facility Dependence in $M6$ Tests

The H_2-fueled scramjet engines were tested under the $M6V$ flight condition and the $M6S$-mode air. The combustion behaviors of scramjet engines were found to be sensitive to the test media, as shown in Table 1 (Ref. 10). In the table, "with preheating" means an ignition test after engine combustion. Therefore, the engine was heated by the burning of the main fuel in advance of the self-ignition test. "Without preheating" implies an engine test condition which self-ignition was tested before engine combustion (therefore, the engine was near the initial temperature of about 300 K). The H_2 selfignited without the assist of the igniters, and so the igniters were not necessary in the $M6V$ cases. However, the selfignition was difficult in the $M6S$ cases. Thus, the vitiated air yielded higher, but false, ignition performance in testing scramjet engines. The easier ignition with the vitiated air may be due to radicals supplied from the combustion heater.[5,10]

The performance of engine thrust was also modified by the test air. The significant difference between the S and the V test air was the maximum fuel rate, which caused the engine unstarted. The engine unstarted at 60 g/s ($\Phi = 0.4$) in the $M6S$ air, and it delivered the largest thrust of 1120 N at 100 g/s ($\Phi = 0.7$) in the $M6V$ air. The dependence of thrust and the unstart criterion on the test air means that the combustion must be partially reaction-controlled in the $M6$ condition, as suggested in Fig. 6.

Heat Flux and Wall Pressure Distributions

The development from the weak combustion mode to the intensive combustion mode was observed by examining the variation of heat flux distribution in the engine. The heat flux distributions along the centerline of the sidewall of the engine are shown in Fig. 7. In Fig. 7, the open triangles represent the heat flux distribution in the fuel-off operation. Initial exothermic reaction, with a fuel flow rate of $\Phi = 0.21$, is detected downstream of the combustor ($x = 1400$ mm), where the shock wave from the cowl impinges. There is no increase of heating rate behind the step in the combustor from 800 to 900 mm in spite of the assistance of the PJ igniters. As the fuel flow rate increases to $\Phi = 0.34$, the heating rate increases and the maximum heating point moves upstream. When the intensive combustion is attained at $\Phi = 0.5$, the combustion is held at the step on the sidewall.

The development of the selfignition-type combustion and the upstream movement of the combustion zone were also confirmed by the wall pressure measurements.[10] With injection of H_2, a high-pressure region appeared downstream of the combustor instead of

behind the backward step. It then moved upstream as the fuel flow rate increased. The pressure pattern suggested that the principal exothermic region was located farther downstream of the step in the combustor. As the fuel flow rate increased, the shock wave due to combustion reached the step and the combustion was anchored there up to the limit value at which the engine unstarted.

Thus, the engine wall pressure and the heat flux distributions indicate that the weak combustion can be approximated by selfignition as observed in the flow reactor experiments, in which the location of the reaction is determined by the balance of the reaction delay time and the flow speed. This is why the ignition properties were sensitive to the reactivity of the test air and the preheating conditions, as shown in Table 1. This reaction-controlled combustion supports the conclusion for the weak combustion described in Fig. 6.

In the intensive combustion, the flame is anchored at the backward-facing step, but it is partially detached from the step on the top wall in the combustor.[10] The detached flame is responsible for the widely scattered data for the $M6$ intensive combustion (open squares) in Fig. 6. The detached flame yields the reaction-controlled combustion to produce the sensitivity to the test air in the $M6$ tests. A similar lack of base-flame holding was reported in expansion ramp injector experiments.[8]

The mixing-controlled combustion found in Fig. 3 suggests the weak facility dependence in the $M8$ combustion. In addition, the amount of residual radicals in our $M8$ facility nozzle (3.4 m long) was as low as 5 ppm, and the residual radicals are negligible in the ignition process. The influences of the air-heating methods on engine performance become weak in the M8 testing in comparison with the M6 engine tests.

Ignition and Combustion in Scramjet Engines

Residence Time in Combustor

In Fig. 8, wall pressure distributions (along the centerline on the side wall) are compared in the engines without struts (solid squares) and with the thick strut (open squares) in the fuel-off condition. The combustion data (solid circles) in the engine with a 46-mm-thick strut are compared with the data without burning. The static pressure at the entrance of the inlet is as low as 4 kPa but increased to 10 kPa in the combustor without the strut (the geometrical compression ratio is 2.86), because the number of reflections of compression waves is limited in the $M8$ condition. Figure 8 shows that installing the thick strut yields a much higher pressure of 50 kPa by means of the higher contraction ratio of 8.3 (open squares). The high-pressure region found around $x = 1300$ mm is caused by impingement of a reattachment shock wave formed at the trailing edge of the thick strut. However, when H_2 is not injected, the wall pressure decays rapidly downstream toward the nozzle.

With combustion, the wall pressure increases drastically in the diverging combustor and the nozzle sections. The pressure distribution indicates that the flame is held behind the strut in the combustor and the main heat release occurs in the diverging combustor section around $x = 1200$ mm, as shown in Fig. 8. To understand the ease of self-ignition or combustion in the flows, environments for reactions in ignition and burning should be discussed.

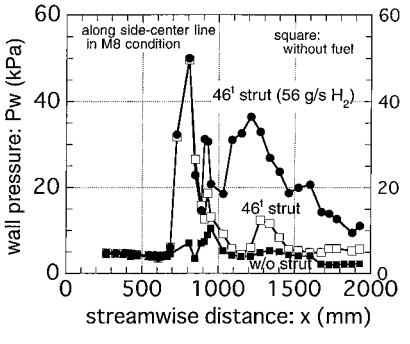

Fig. 8 Distributions of wall pressure with various struts in the $M8$ condition.

An averaged static pressure for reactions is defined as

$$\bar{P} = \left\{ \int_0^{x_e} P_w(x)^n \cdot \frac{dx}{x_e} \right\}^{1/n} \tag{3}$$

where the static pressure is represented with the wall pressure (P_w) and x_e denotes the combustible flow length from the backward-facing step to the exit of engines (1.3 m). The exponent, n, can be determined by overall reaction for ignition and combustion. An averaged Mach number can be evaluated by assuming loss in the total pressure, then the flow velocity and the residence time of reactants in the engine are calculated. The flow velocity is estimated using the preignition condition with $n = 1$ in Table 2.

Mach number in engines depends on the engine configuration and combustion. Mounting of the larger struts increases the compression ratios of the engine and reduces the flow Mach numbers. The typical Mach number in the combustion region from the combustor to the nozzle exit was found to be 2 for the strutless engine in the $M4$ condition and to vary from about 4 to 2 in the $M6$ case. The Mach number in the $M8$ tests were chosen to be from $M = 5$ to $M = 3$. Table 2 shows that the flow velocity varies from nearly 900 m/s in the $M4$ case to more than 2,000 m/s in the $M8$ case. Corresponding to these velocities, the residence time in the combustion region ranges between 1 ms (the $M4$) to 0.5 ms (the $M8$).

Ignition Time in Engine

To compare this residence, the ignition delay time and the burning time must be estimated. Four sets of reaction rate data in Refs. 2, 3, 19, and 20 were compared in this study. The comparison showed that the shortest ignition delay time was obtained with the data used by Rogers and Schexnayder[2] and the longest delay time was found with the kinetics cited in Ref. 19. However, the difference was smaller than 20% at most in a higher pressure of 100 kPa. There was no significant difference in the burning time, except for the result using Jachimowski's data.[3] The reaction rate of a reaction $2O \rightarrow O_2$ in Ref. 3 might be overestimated. Therefore, the rate constants adopted in Ref. 2 were used in this study.

The ignition delay in H_2–air reactions is governed by a branching reaction: $H + O_2 \rightarrow OH + H$ (called the R_1 reaction) with the rate of $k_1[O_2][H]$. A numerical study by Rogers and Schexnayder[2] showed that experimental data on ignition could be correlated with the time required to raise the temperature by 5% of total temperature increment by combustion ($t_{5\%}$). We found that the $t_{5\%}$ was approximated by $10 \times t_1$, and it is here labeled as t_{ig}. Therefore, the reaction time for self-ignition is given as

$$t_{ig} = 10 \times t_1, \qquad t_1 = (k_1 \times [O_2])^{-1}$$

$$k_1 = 1.25 \times 10^{14} \exp(-8450/T_r) \tag{4}$$

This result implies that the reaction pressure can be averaged with $n = 1$ in Eq. (3) because the ignition reaction rate is proportional to P^1. The t_{ig} is illustrated by solid lines in Fig. 9. Because the temperature dependence of R_1 is strong, the ignition delay time rapidly increases if reaction temperature lowers below 1000 K. This implies

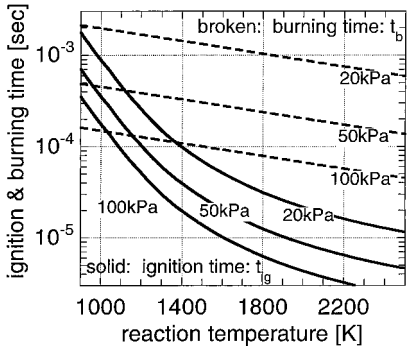

Fig. 9 Ignition time and combustion time in scramjet conditions.

that self-ignition is possible only in the boundary layer or the recirculation zones behind the struts where the temperature can recover.

Maximum temperature in the boundary layer in the engine was investigated to identify the probable ignition points. The maximum temperature in the isothermal boundary layer on the water-cooled engine (wall temperature = 400 K) was evaluated to be 600 K for the $M6$ case. The temperature is not enough for the autoignition in the engines. However, our numerical simulation studies showed that the recirculation zone behind the struts provided a hot region where gas temperature recovered to near the adiabatic value even for the isothermal wall. In the $M8$ and $M6$ experiments, some thermocouples detected local ignition at the backward-facing steps, behind the strut and near the cowl leading edge. These facts suggest that some narrow regions near the step and the strut are heated to the adiabatic recovery temperature to initiate combustion in the engines. The adiabatic recovery temperatures (T_r) are listed in Table 2.

Using the recovery temperature with the average pressure of $P_i = 29$ kPa, Table 2 illustrates that the ignition delay length given by $x_{ig} = U \times t_{ig}$ becomes 2.13 m in the $M4$ case. The ignition length surpassing the engine length shows that the residence time is insufficient to ignite reactants, and some forced ignition device is required in the $M4$ condition. The recovery temperature increases to 138 K in the $M6$ case, and the ignition delay length becomes $\frac{1}{10}$ of that in the $M4$ case. The engine condition was found to be on the boundary of the self-ignition limit for both the S and V modes, and the engine could self-ignite without the PJ igniters in the $M6V$ case and sometimes in the $M6S$ case. The solid triangle data in Fig. 6 support this observation. The ignition delay length is shortened considerably in the $M8$ condition because of the higher T_r of 2400 K. Reactions are accelerated so that the actual ignition is now governed by the mixing of H_2.

Burning Times in Engines

Combustion is controlled by a reaction mechanism different from that in ignition. Rogers and Schexnayder[2] proposed an empirical burning time through chemical kinetic. The burning time, following the self-ignition, was defined as the time to raise the temperature from 5% to 95% of the equilibrium temperature rise. The burning time (s) is presented as a function of pressure (P in atm) and the initial temperature, denoted as T_r here,

$$t_{95} = 3.25\text{E}{-4} \times \text{P}^{-1.6} \times \exp(-0.8 \times T_r/1000) \qquad (5)$$

The reaction time is labeled as the burning time (t_b) and is plotted in Fig. 9. The weak temperature dependence and the strong pressure dependence of t_b are attributed to the partial equilibrium of radicals. As a consequence, these dependences pose a significant problem in scramjet engines. Figure 9 shows that the overall combustion time is governed by the ignition delay below 1000 K, but it is controlled by the burning time above 1200 K. For instance, the burning requires the reaction time (t_b) longer than t_{ig} by 50 times in 20 kPa, even in the case of this infinitely fast mixing limit. Since t_b indicates the pressure dependence proportional to $\text{P}^{-1.6}$, the burning pressure should be averaged by using Eq. (3) with $n = 1.6$. The average reaction pressure for burning is summarized as P_b in Table 2.

The burning pressure is high ($P_b = 85$ kPa) in the $M4$ burning condition, and so the burning time and the burning distance are evaluated to be 220 μs and 0.19 m. Therefore, the combustion can be completed in the combustor if the combustion was initiated. Unfortunately, however, ignition and flame propagation were difficult in the $M4$ condition. Complete combustion was possible only near the top wall, where the PJ igniters were attached. This supports the experimental result of high η_c near the top wall shown in Fig. 5.

In the $M6$ condition, the engine in the weak combustion with the $1/5H$ strut requires a long burning distance of 1.7 m. Gas sampling detected large amounts of unburned H_2 in the weak combustion.[10] In the intensive combustion, the engines with the $1/5H$ and the $5/5H$ struts sustain sufficient pressure for combustion reactions (64–69 kPa). The shorter length for burning of 0.3 to 0.2 m is required in the intensive combustion. Vigorous combustion resulted in bulk η_c of about 90% in the $M6$ intensive combustion.

Table 2 shows that the engine without struts requires a burning distance of 6 m in the $M8$ condition, because the reaction pressure was as low as $P_b = 7.9$ kPa. Consequently, the $M8$ engine tests frequently had the unburnt H_2 exhausted from the engine nozzle, which then ignited and burned in the facility diffuser connected to the test cell. Attaching the thick $5/5H$ strut increased P_b to 24 kPa and shortened the x_b to 0.84 m. Combustion then became possible inside the engine. This was consistent with the combustion with the high η_c depicted in Fig. 2a.

However, the reaction in the $M8$ engine condition is not so fast as in the $M6$ case. The main combustion region might be blown downstream. This suggests that a small pressure increase may move the combustion zone upstream to locate the high-pressure region near the strut and then produce a further pressure increase (a favorable loop). Figure 8 illustrates that the high pressure caused by combustion is located around $x = 1{,}300$ mm in the middle reach of the diverging section. If the high-pressure region can be shifted upstream by designs optimizing struts, the thrust performance of the engine can be improved even when fairly high η_c has been achieved at the engine exit.[15]

Conclusions

To understand the facility dependence found in the $M6$ engine testing, rate processes governing combustion in scramjet engines were investigated by use of gas sampling, wall pressure, and heating rate data in engine tests. The correlation between the local equivalence ratio and the local combustion led to the following conclusions:

1) The $M4$ combustion was principally reaction controlled, and the reaction- and the mixing-controlled combustion coexisted in the engine in the $M6$ condition. Combustion in the engine with the thick strut was rate controlled by the mixing of H_2 in the $M8$ tests.

2) The wall-heating rate and pressure distributions suggested switching from the reaction-controlled to the mixing-controlled combustion with increasing fuel rate in the $M6$ tests.

3) The sensitivity of engine performance to the storage-heated and vitiation-heated air could be explained with the partially reaction-controlled combustion in engines in the $M6$ tests.

4) Pressure for reactions for ignition and combustion was investigated to estimate the ease of autoignition and burning under the scramjet engine conditions. The reaction is not sufficiently fast in the $M8$ engine condition compared with that in the $M6$ case. The main combustion region might be blown downstream in the engine.

Acknowledgment

The authors thank Tetsuo Hiraiwa for useful discussion on chemical kinetics and reduces kinetics for scramjet combustion.

References

[1]Carson, G. T., Jr., "Analytical Chemical Kinetic Investigation of the Effects on Oxygen, Hydrogen, and Hydrooxyl Radicals on Hydrogen-Air Combustion," NASA TN-D-7769, 1974.

[2]Rogers, R. C., and Schexnayder, C. J., "Chemical Kinetic Analysis of Hydrogen-Air Ignition and Reaction Times," NASA TP 1856, 1981.

[3]Jachimowski, C. J., "An Analytical Study of the Hydrogen-Air Reaction Mechanism with Application to Scramjet Combustion," NASA TP 2791, 1988.

[4]Srinivasan, S., and Erickson, W., "Interpretation of Vitiation Effects on Testing at Mach 7," AIAA Paper 95-2719, July 1995.

[5]Mitani, T., "Ignition Problems in Scramjet Testing," *Combustion and Flame*, Vol. 101, 1995, pp. 347–359.

[6]Guy, R. W., Rogers, R. C., Puster, R. L., Rock, K. E., and Diskin, G. S., "The NASA Langley Scramjet Test Complex," AIAA Paper 96-3243, July 1996.

[7]Northam, G. B., "Report on Combustion in Supersonic Flow," *Proceedings of the 21st JANNAF Comb. Meeting*, Chemical Propulsion Information Agency, 1984, pp. 399–410.

[8]Rogers, R. C., Capriotti, D. P., and Guy, R. W., "Experimental Supersonic Combustion Research at NASA Langley," AIAA Paper 98-2506, June 1998.

[9]Chinzei, N., Mitani, T., and Yatsuyanagi, N., "Scramjet Engine Research at National Aerospace Laboratory, Japan," *Progress in Astronautics and Aeronautics*, in printing, AIAA, 2000.

[10]Mitani, T., Hiraiwa, T., Sato, S., Tomioka, S., Kanda, T., and Tani, K., "Comparison of Scramjet Engine Performance in Mach 6 Vitiated and Storage-Heated Air," *Journal of Propulsion and Power*, Vol. 13, No. 5, 1997, pp. 635–642.

[11]Kanda, T., Hiraiwa, T., Mitani, T., Tomioka, S., and Chinzei, N., "Mach 6 Testing of a Scramjet Engine model," *Journal of Propulsion and Power*, Vol. 13, No. 4, 1997, pp. 543–551.

[12]Hiraiwa, T., Sato, S., Tomioka, S., Kanda, T., Shimura, T., and Mitani, T., "Testing of a Scramjet Engine Model in Mach 6 Vitiated Air Flow," AIAA Paper 97-0292, Jan. 1997.

[13]Mitani, T., Chinzei, N., and Masuya, G., "M2.5 Experiments of Reaction Quenching in Gas Sampling for Scramjet Engines," *Proceedings of the 27th International Symposium on Combustion*, Combustion Institute, Pittsburgh, PA, 1998, pp. 2151–2156.

[14]Mitani, T., Takahashi, M., Tomioka, S., Hiraiwa, T., and Tani, K., "Analyses and Application of Gas Sampling to Scramjet Engine Testing," *Journal of Propulsion and Power*, 1999, pp. 572–577.

[15]Kanda, T., Wakamatsu, Y., Ono, F., Kudo, K., Murakami, A., and Izumikawa, M., "Mach 8 Testing of a Scramjet Engine Model," AIAA Paper 99-0617, Jan. 1999.

[16]Saito, T, Wakamatsu, Y., Mitani, T., Chinzei, N., and Shimura, T., "Mach 8 Testing of a Scramjet Engine Model," *Proceedings of the 20th International Symposium on Space Technology and Science*, Gifu, Japan, 1996, pp. 58–63.

[17]Tomioka, S., Kanda, T., Tani, K., Mitani, T., Shimura, T., and Chinzei, N., "Testing of a Scramjet Engine with a Strut in M8 Flight Conditions," AIAA Paper 98-3134, July 1998.

[18]Sunami, T., Sakuranaka, N., Tani, K., Hiraiwa, T., and Shimura, T., "Mach 4 Tests of a Scramjet Engine—Effects of Isolator," *Proceedings of the 13th International Symposium on Air Breathing Engines*, 1997, pp. 615–625.

[19]Radhakrishnan, K., and Bittker, D. A., LSENS, *A General Chemical Kinetics and Sensitivity Analysis Code for Homogeneous Gas-Phase Reactions*, NASA Reference Publication 1329, 1994.

[20]Balakrishnan, G., and Williams, F. A., "Turbulent Combustion Regimes for Hypersonic Propulsion Employing Hydrogen–Air Diffusion Flames," *Journal of Propulsion and Power*, Vol. 10, No. 3, 1994, pp. 434–437.